Quantitative Shape Measurement of an Inflatable Rubber Dam Using an Array of Inertial Measurement Units

Authors: Yonghui Hu [a]

Yong Yan [a] (Corresponding author)

Christos Efstratiou [a]

David Vela-Orte [b]

Addresses: [a] School of Engineering and Digital Arts

University of Kent

Canterbury

Kent CT2 7NT

UK

Tel: 00441227823015

Fax: 00441227456084

Email: y.yan@kent.ac.uk

[b] Dyrhoff Limited

Folkestone

Kent CT19 4RJ

UK

ABSTRACT

Shape measurement plays an important role in the condition monitoring and operation control of inflatable rubber dams. This paper presents a method to measure the cross-sectional shape of a rubber dam using an array of inertial measurement units (IMUs) placed on the circumference of the dam. Accelerometer and gyroscope measurements are combined using an adaptive complementary filter to determine the tangent angles of the dam circumference. The adaptive complementary filter adjusts the weights of the accelerometer and gyroscope measurements dynamically in order to reduce the uncertainty in orientation estimation due to external acceleration under dynamic conditions. A natural cubic spline that interpolates the measured tangent angles at discrete locations is used to represent the tangent angles along the dam circumference as a continuous function of the arc length. Finally, the cross-sectional shape is reconstructed by integrating the continuous tangent angle function along the circumference of the dam. Experimental assessment of the measurement system was performed on a purpose-built test rig using a digital camera as a reference measuring device. Results under a typical static condition show that the measured and reference shapes agree well with each other, with a similarity index of 3.74%, mismatch distance of the last IMU node being 12.3 mm and relative error of height measurement being -2.44%. Under dynamic conditions, the measurement results deteriorate due to external acceleration, but considerable improvement is achieved in comparison with an accelerometer-only approach. In addition, elimination of faulty nodes from shape reconstruction has negligible influence on the results, suggesting that the measurement system enjoys a high degree of fault tolerance.

Keywords – Inflatable rubber dam, shape measurement, inertial measurement unit (IMU), adaptive complementary filter, tangent angle, natural cubic spline.

I. INTRODUCTION

Inflatable rubber dams are flexible cylindrical structures for control of water level and flow in rivers and waterways [1]. They can be inflated by air, water or a combination of both to raise the upstream water level and partially or completely deflated to release the impounded water, working as crest-adjustable water gates. In comparison with traditional rigid hydraulic structures such as earth and concrete weirs, rubber dams provide a number of advantages, including low cost, simple structure, short construction time, easy maintenance and repair, more earthquake resistant and environmentally friendly. Since 1950s, thousands of rubber dams have been constructed around the world for various purposes, such as irrigation, water supply, hydropower generation, tidal barrier, flood control, recreation, etc.

The benefits associated with the flexibility of the rubber dam structure are accompanied by significant challenges in their design and operation. The cross-sectional shape and height of a rubber dam vary continuously with external water levels and internal pressures, while the forces applied externally and internally depend in turn on the dam shape and height [2]. The two-way interaction between loading and shape calls for complex mathematical models for design and analysis as well as continuous monitoring and control of the dam shape and height. Knowledge about the dam shape provides key information about the condition of the rubber dam, such as the V-notch phenomenon of air-filled dams and the dam height that determines the upstream reservoir level. In addition, rubber dams are subject to a wide variety of disturbances such as water waves, overflow and impact of passing debris, which result in vibration of the dam body [3]. Long-term excessive vibration leads to wear and delamination of the membrane material and even premature failure of the rubber dam. It is therefore desirable to monitor the dam vibration, so that countermeasures such as adjustment of the internal pressure can be taken to suppress the vibration.

This study aims to develop a smart condition monitoring system that measures the cross-sectional shape, height and vibration of rubber dams. To the best of our knowledge, there is no prior research on this topic in the rubber dam sector. Typically, rubber dams vibrate at frequencies below 1 Hz. If the shape of the rubber dam can be measured continuously, vibration parameters such as vibration frequency and amplitude can be derived from the animated shape. The height of the rubber dam can also be easily determined by locating the peak point in the shape. Consequently, this paper focuses on continuous measurement of the cross-sectional shape.

A number of techniques based on different sensing principles have been developed in the past to measure the shape of structures. Non-contact methods based on stereo vision and structured light can reconstruct complex three-dimensional (3D) shapes with high resolution and high speed [4, 5], but these systems require installation of multiple cameras or controlled lighting conditions, which are difficult to implement in the field. Fiber Bragg grating (FBG) sensors have received considerable interests in recent years for shape measurement of wind turbine blades, aircraft wings, soft robots and high-voltage power transmission lines due to advantages of small size, light weight, immunity to electromagnetic interference, resistance to corrosion, and multiple measuring points in one optical fiber [6-8]. However, the high cost, adverse temperature effects and sophistication of the system make this technique not well suited for the intended application in this study. Resistive flex and stretch sensors that are extensively used in wearable devices can measure bending or flexing based on the resistance across the sensor [9, 10]. Although they are simple, cheap, compact and robust, shortcomings such as nonlinearity, lower sensitivity, low accuracy and limited length restrict wider application of this technology. Accelerometers are widely used to determine the inclination or tilt angles by sensing the gravity. An array of accelerometers attached to the measured object can provide local inclination information for

global shape reconstruction. A number of studies have used this technique for measurement of human spine postures and 3D shape sensing of flexible materials [11-15]. The developments of microelectromechanical-systems (MEMS) technology in the last decade have produced many low cost, small size, light weight and readily available accelerometers. In this study, MEMS accelerometers are considered best-suited for shape measurement of rubber dams among all the techniques reviewed.

As aforementioned, rubber dams are prone to vibrate due to external excitation. Under such dynamic conditions, accelerometer measurements are easily corrupted by external acceleration, leading to large measurement errors of the inclination. Theoretically, it is an underdetermined problem to separate the gravitational acceleration and the external acceleration from the accelerometer signal, which is the sum of both components. Several studies have been conducted to compensate for external acceleration using MEMS gyroscopes and sensor fusion algorithms augmented by adaptation mechanisms [16-24]. The angular rate measured by a gyroscope can be integrated to provide an estimate of the orientation angle. However, MEMS gyroscopes suffer from low-frequency drift and bias, which result in unbounded accumulation errors in long-term monitoring. Nevertheless, it is well accepted that gyroscope and accelerometer measurements can be fused together to achieve better orientation estimates in dynamic conditions. Several sensor fusion methods have been developed in the literature, among which Kalman filter [16-18] and complementary filter [19-24] are most widely used. Kalman filter recursively predicts and corrects the orientation estimates using gyroscope and accelerometer measurements, respectively. It is an optimal state estimator in the sense of minimal mean square error but requires knowledge of the system model and noise characteristics. The complementary filter combines the low-frequency components of the accelerometer measurements and the high-frequency components of

the gyroscope measurements, which are reliable under quasi-static and dynamic conditions, respectively. In comparison with Kalman filter, the complementary filter is simple, easy to implement and computationally efficient. In order to deal with external acceleration, different adaptation schemes have been proposed to augment both Kalman and complementary filters [16-24]. The fundamental idea of these methods is to tune the filter gain parameters adaptively according to the magnitude of external acceleration. In static and quasi-static conditions, accelerometer measurements are given relatively larger weight in the sensor fusion algorithm, while the gyroscope is more trustworthy under circumstances of large external acceleration.

The basic concept of shape measurement of rubber dams using inertial sensors along with preliminary experimental results was first reported in 2020 at the IEEE International Instrumentation and Measurement Technology Conference [25]. This paper presents in detail the fundamental principle, practical design and implementation, and experimental assessment of the measurement system under both static and dynamic conditions. In particular, an adaptive complementary filter algorithm is designed to address the problematic external acceleration under dynamic conditions.

II. MEASUREMENT PRINCIPLE AND SYSTEM DESIGN

A. Overall Sensing Arrangement

A rubber dam is made of a sheet of rubber-coated fabric that is fixed to a reinforced concrete foundation using clamp plates and anchor bolts. When inflated, the rubber dam forms a shape of a teardrop, which depends on the internal pressure, upstream and downstream water depths. When completely deflated, the rubber membrane flattens onto the rigid foundation. The height of the largest rubber dam in the world reaches 6 m, while for majority of the rubber dams the height is

less than 3 m. A number of analytical and numerical methods have been developed to determine the cross-sectional shape of a rubber dam under given conditions [2, 26]. Fig. 1 illustrates the typical shape of a rubber dam with two clamping lines.

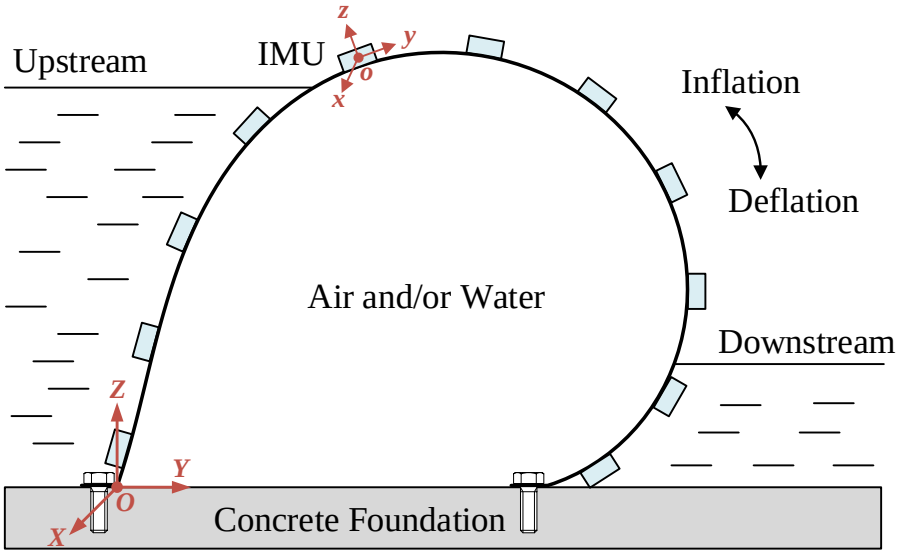

Fig. 1. Placement of the IMU array on the rubber dam.

An electronic device that integrates a tri-axis accelerometer, a tri-axis gyroscope and a sensor fusion algorithm running on a microcontroller is known as an inertial measurement unit (IMU). In order to measure the shape of the rubber dam, an array of IMUs with known distance between adjacent nodes is placed on the circumference of the rubber dam. Using the tangent angles measured by the IMUs, the cross-sectional shape of the rubber dam can be reconstructed numerically using some appropriate algorithm. Fig. 1 illustrates the overall sensing arrangement and principle of the measurement system. It should be noted that the placement of the IMU array on the rubber dam cause negligible change to the shape of the rubber dam, because the IMUs are light-weight and very small-size in comparison with the target. In addition, the nodes of the IMU array are not necessarily equidistant, which implies that outlier readings of faulty nodes can be removed from the shape reconstruction algorithm without inducing significant errors.

B. ***Tangent Angle Measurement***

The tangent angle of the rubber dam at the IMU location can be described by a rotation angle from an earth-fixed coordinate frame *O-XYZ* to an IMU-fixed coordinate frame *o-xyz*, as illustrated in Fig. 1. The rotation between two coordinate frames can be represented by Euler angles, a direction cosine matrix (DCM) or a quaternion [24]. Because of the singularity problem of Euler angles and the high computational cost of DCM differential equations, the quaternion representation is used to calculate the orientation angles. A quaternion can be regarded as a four-element vector, with the first element denoting the scalar part and the second to last elements comprising the vector part [18]. Rotation about a unit vector $\boldsymbol{v} = [v_x \; v_y \; v_z]^T$ by an angle θ is represented by the following unit quaternion:

$$q = \begin{bmatrix} q_0 \\ q_1 \\ q_2 \\ q_3 \end{bmatrix} = \begin{bmatrix} \cos\dfrac{\theta}{2} \\ v_x \sin\dfrac{\theta}{2} \\ v_y \sin\dfrac{\theta}{2} \\ v_z \sin\dfrac{\theta}{2} \end{bmatrix} \tag{1}$$

Let $a = [a_x \; a_y \; a_z]^T$ denote the gravitational vector in the IMU-fixed coordinate frame and $g = [0 \; 0 \; 1]^T$ the normalized gravitational vector in the earth-fixed coordinate frame, respectively. The rotation angle θ_a between the two frames can be found from the dot product of the two vectors:

$$a \cdot g = \|a\| \|g\| \cos\theta_a \tag{2}$$

which yields:

$$\theta_a = \cos^{-1}\left(\frac{a \cdot g}{\|a\|\|g\|}\right) = \cos^{-1}\left(\frac{a_z}{\sqrt{a_x^{\,2} + a_y^{\,2} + a_z^{\,2}}}\right) \tag{3}$$

where a_x, a_y and a_z are the outputs of the tri-axis accelerometer. Meanwhile, the rotation axis v_a can be determined using the cross product of the two vectors:

$$v_a = a \times g = \begin{bmatrix} a_y \\ -a_x \\ 0 \end{bmatrix} \tag{4}$$

Therefore, the orientation q_a measured by the accelerometer can be expressed in unit quaternion form as:

$$q_a = \begin{bmatrix} q_{a0} \\ q_{a1} \\ q_{a2} \\ q_{a3} \end{bmatrix} = \begin{bmatrix} \cos\dfrac{\theta_a}{2} \\ \dfrac{a_y}{\sqrt{a_x^{\,2} + a_y^{\,2}}} \sin\dfrac{\theta_a}{2} \\ \dfrac{-a_x}{\sqrt{a_x^{\,2} + a_y^{\,2}}} \sin\dfrac{\theta_a}{2} \\ 0 \end{bmatrix} \tag{5}$$

Assuming that the gyroscope measurement is drift-free and noiseless, orientation measurement can be achieved by solving the following quaternion kinematic differential equation according to the angular velocity measured by the gyroscope [18]:

$$\dot{q}_g = \frac{1}{2} q_g \otimes \boldsymbol{p}(\omega) \tag{6}$$

where $q_g = [q_{g0}\ q_{g1}\ q_{g2}\ q_{g3}]^T$ is a unit quaternion representing the orientation derived using the gyroscope, $\otimes$ is the quaternion product operator, $\omega = [\omega_x\ \omega_y\ \omega_z]^T$ represents the outputs of the tri-axis gyroscope, and $\boldsymbol{p}(\square)$ converts a vector to a pure quaternion, i.e. $\boldsymbol{p}(\omega) = [0\ \omega_x\ \omega_y\ \omega_z]^T$. Substituting the expressions of q_g and $\boldsymbol{p}(\omega)$ into equation (6) and solving the resulting

differential equation using the first-order Runge-Kutta method yield the following recursive update equation in discrete form:

$$\begin{bmatrix} q_{g0,k} \\ q_{g1,k} \\ q_{g2,k} \\ q_{g3,k} \end{bmatrix} = \begin{bmatrix} q_{g0,k-1} \\ q_{g1,k-1} \\ q_{g2,k-1} \\ q_{g3,k-1} \end{bmatrix} + \frac{\Delta t}{2} \begin{bmatrix} 0 & -\omega_x & -\omega_y & -\omega_z \\ \omega_x & 0 & \omega_z & -\omega_y \\ \omega_y & -\omega_z & 0 & \omega_x \\ \omega_z & \omega_y & -\omega_x & 0 \end{bmatrix} \begin{bmatrix} q_{g0,k-1} \\ q_{g1,k-1} \\ q_{g2,k-1} \\ q_{g3,k-1} \end{bmatrix} \tag{7}$$

As discussed, the accelerometer and gyroscope have complementary characteristics in the frequency domain. The orientation estimates from the accelerometer and gyroscope can be viewed as noisy versions of the true orientation corrupted by high- and low-frequency noises, respectively. Therefore, the true orientation can be estimated more accurately if the two estimates are combined after they pass through a low- and a high-pass filter, respectively, which share the same cut-off frequency. In the time domain, the orientation estimated using the accelerometer and gyroscope can be fused using the following linear complementary filter:

$$q = \gamma q_a + (1-\gamma) q_g \tag{8}$$

where γ is a weight coefficient, which lies between 0 and 1. In equation (7), the recursive update operation using the angular velocity leads to unbounded accumulation error due to gyroscope drift. To eliminate the steady-state error, the fused orientation estimate is used to update the gyroscope estimate, which gives the following update equation:

$$\begin{bmatrix} q_{0,k} \\ q_{1,k} \\ q_{2,k} \\ q_{3,k} \end{bmatrix} = \gamma \begin{bmatrix} q_{a0,k} \\ q_{a1,k} \\ q_{a2,k} \\ q_{a3,k} \end{bmatrix} + (1-\gamma) \begin{bmatrix} q_{0,k-1} \\ q_{1,k-1} \\ q_{2,k-1} \\ q_{3,k-1} \end{bmatrix} + \frac{(1-\gamma)\Delta t}{2} \begin{bmatrix} 0 & -\omega_x & -\omega_y & -\omega_z \\ \omega_x & 0 & \omega_z & -\omega_y \\ \omega_y & -\omega_z & 0 & \omega_x \\ \omega_z & \omega_y & -\omega_x & 0 \end{bmatrix} \begin{bmatrix} q_{0,k-1} \\ q_{1,k-1} \\ q_{2,k-1} \\ q_{3,k-1} \end{bmatrix} \tag{9}$$

The linear complementary filter with a fixed weight coefficient cannot yield reliable orientation estimates over a wide range of dynamic conditions. In order to compensate for the varying

external acceleration, the weight coefficient is adjusted dynamically according to the following adaptation law:

$$\gamma = e^{\lambda\left|\|\boldsymbol{a}\|-G\right|} \tag{10}$$

where G is the gravitational constant and λ is a negative constant that determines the decay rate. Equation (10) suggests that the weight coefficient decreases exponentially when the magnitude of the measured acceleration differs from the gravitational constant, giving more credibility to the gyroscope. While in static conditions, the weight coefficient equals 1 and the measurement relies solely on the accelerometer. Fig. 2 shows a block diagram of the adaptive complementary filter.

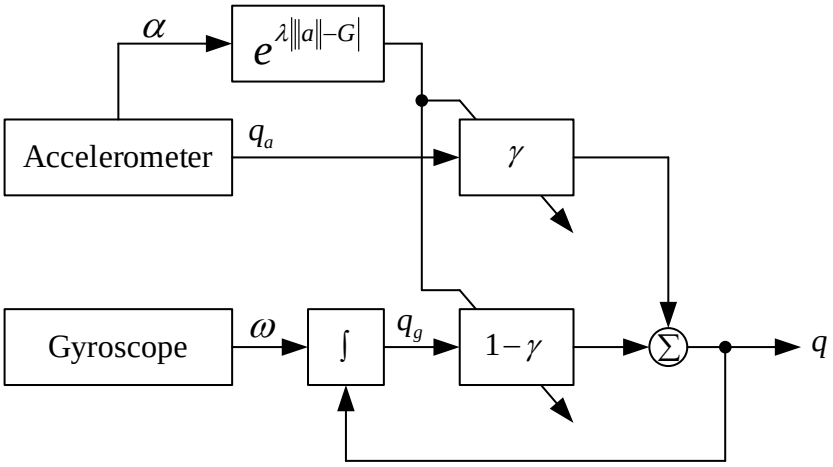

Fig. 2. Block diagram of the adaptive complementary filter.

As illustrated in Fig. 1, the earth-fixed coordinate frame *O*-*XYZ* is defined in such a way that its *Y*-axis points from the upstream to the downstream side, the *Z*-axis points upward, and the *X*-axis is aligned with the longitudinal direction of the rubber dam and follows the right-hand rule. Following such a definition, the tangent angle of the rubber dam can be represented by the roll angle ϕ of the IMU, which is derived from the orientation quaternion as:

$$\phi = \mathrm{tg}^{-1}\frac{2(q_2q_3 + q_0q_1)}{1-2({q_1}^2 + {q_2}^2)} \tag{11}$$

The roll angle lies in the range of -180 ºto 180 º.

C. ***Shape Measurement***

According to the theory of classical differential geometry [27], the cross-sectional shape of the rubber dam can be described by a differentiable curve in the *YZ*-plane of the earth-fixed coordinate frame *O-XYZ*, as illustrated in Fig. 1. The differentiable plane curve, if parameterized by the arc length, is a differentiable map $\alpha: [0, L] \to \mathbb{R}^2$ given by $\alpha(s) = [y(s), z(s)]$, where L is the peripheral length of the rubber dam, and s is the arc length measured from the origin of the earth-fixed coordinate frame *O-XYZ*, which corresponds to the anchor point at the upstream side in Fig. 1. The tangent vector of the curve $\alpha(s)$ at arc length s is defined by the derivative of the parameterization variable:

$$\begin{aligned} \alpha'(s) &= [\frac{dy(s)}{ds}, \ \frac{dz(s)}{ds}] \\ &= [\cos\phi(s), \ \sin\phi(s)] \end{aligned} \tag{12}$$

which is a unit vector making an angle $\phi(s)$ with the *Y*-axis, as shown in Fig. 3(a). It is clear that the tangent angle $\phi(s)$ varies continuously on the circumference of the rubber dam.

The tangent angle ϕ_i measured at s_i by the *i*-th (i = 1, 2, …, n) IMU can be regarded as a sample of the continuous tangent angle function $\phi(s)$, where n is the total number of IMUs. Polynomial-based interpolation methods construct an approximate function by fitting the known data points to a linear combination of polynomials. In this study, a natural cubic spline that interpolates the discrete measurement points with piecewise third-order polynomials is used to represent $\phi(s)$ [15], as shown in Fig. 3(b). The first and second derivatives of a cubic spline are continuous at the knots, which guarantees the smoothness of the curve. The following equation describes the natural cubic spline:

$$\phi(s)=\begin{cases}\phi^{(1)}(s)=a_1s^3+b_1s^2+c_1s+d_1, & s_1\le s\le s_2\\ \vdots & \\ \phi^{(n-1)}(s)=a_{n-1}s^3+b_{n-1}s^2+c_{n-1}s+d_{n-1}, & s_{n-1}\le s\le s_n\end{cases} \tag{13}$$

which satisfies $\phi^{(i-1)}(s_i)=\phi^{(i)}(s_i)$, $\phi^{(i-1)\prime}(s_i)=\phi^{(i)\prime}(s_i)$, $\phi^{(i-1)\prime\prime}(s_i)=\phi^{(i)\prime\prime}(s_i)$ and $\phi^{(1)\prime\prime}(s_1)=\phi^{(n-1)\prime\prime}(s_n)=0$.

Once the analytical expression of $\phi(s)$ is obtained, the curve can be reconstructed by integrating the tangent vector:

$$\alpha(s)=[\int_0^s\cos\phi(t)dt,\ \int_0^s\sin\phi(t)dt] \tag{14}$$

A number of numerical integration methods based on different rules, such as midpoint, trapezoidal and Simpson's rules, are available to compute numerical approximation to the coordinates of the curve in the *YZ* plane. Fig. 3(a) illustrates an example of shape reconstruction using the above algorithm.

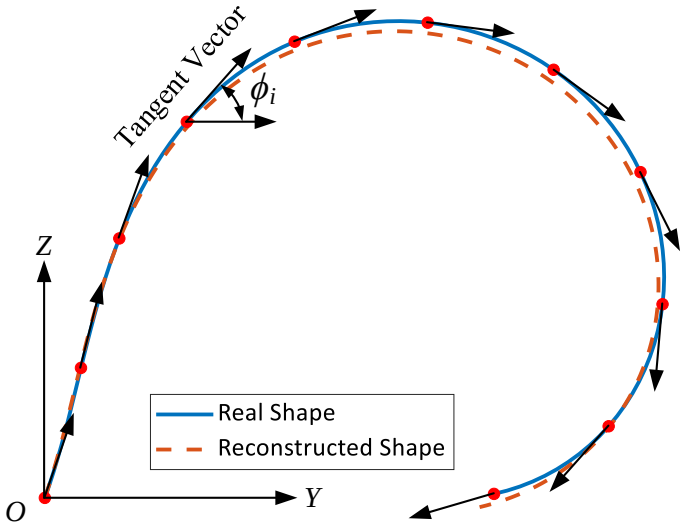

(a) Real and reconstructed shapes.

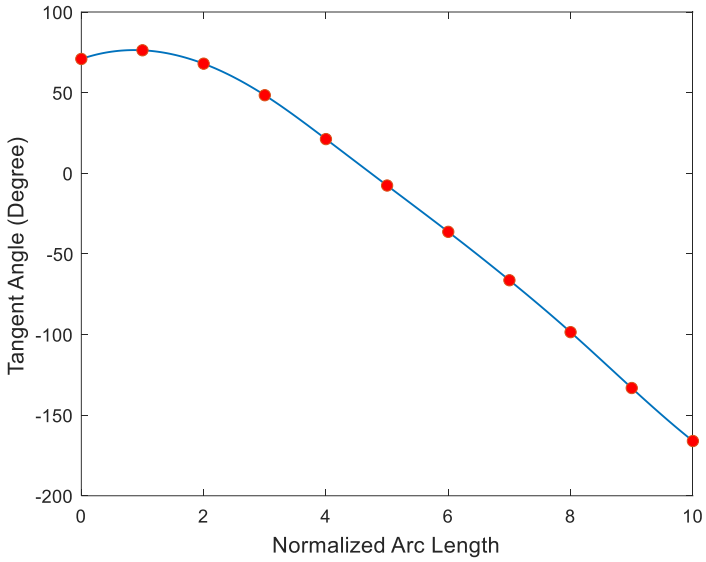

(b) Interpolation of the tangent angles using a natural cubic spline. The distance between adjacent IMUs is normalized as 1.

Fig. 3 Reconstruction of the cross-sectional shape.

As can be seen from the example in Fig. 3(a), the reconstructed shape differs slightly from the real one. The main reason for the error is that the continuous tangent angle function $\phi(s)$ established using tangent angles ϕ_i at discrete locations is only an approximation of the real one. The error can be reduced by increasing the number of IMUs, which leads to a more accurate approximation of the real tangent angle function. In addition, approximation errors are induced when solving equation (14) through numerical integration. In practice, the noise in sensor readings is passed down through the IMU array and the errors of orientation estimate are accumulated, because the coordinates of the *i*-th IMU node are established upon those of the (*i*-1)-th node, resulting in an increasing error in the shape measurement from the first to the last node.

D. ***System Design and Implementation***

The measurement system consists of an IMU array and a host PC that are serially connected by a RS485 bus and a power cable, as illustrated in Fig. 4. The number of IMUs depends on the peripheral length of the rubber dam and the desired accuracy of shape reconstruction. A USB-to-

RS485 converter allows the IMUs to be connected to and powered by an USB port of the PC. The Modbus RTU protocol is used for master-slave communication between the PC and IMUs. In dynamic conditions, IMU readings at the same instant should be used for shape reconstruction. To achieve this, the PC sends out a broadcast command to prompt simultaneous storage of the measurement results on all IMUs, which are then collected successively by the PC. A console program that communicates with the IMUs, implements the shape measurement algorithm and visualizes the reconstructed shape on the PC was developed using Microsoft Visual C# .NET. For industrial applications, the IMU array will be connected to an on-site programmable logic controller (PLC) instead of a PC. The shape measurement results are then used for fault detection and control of the rubber dam.

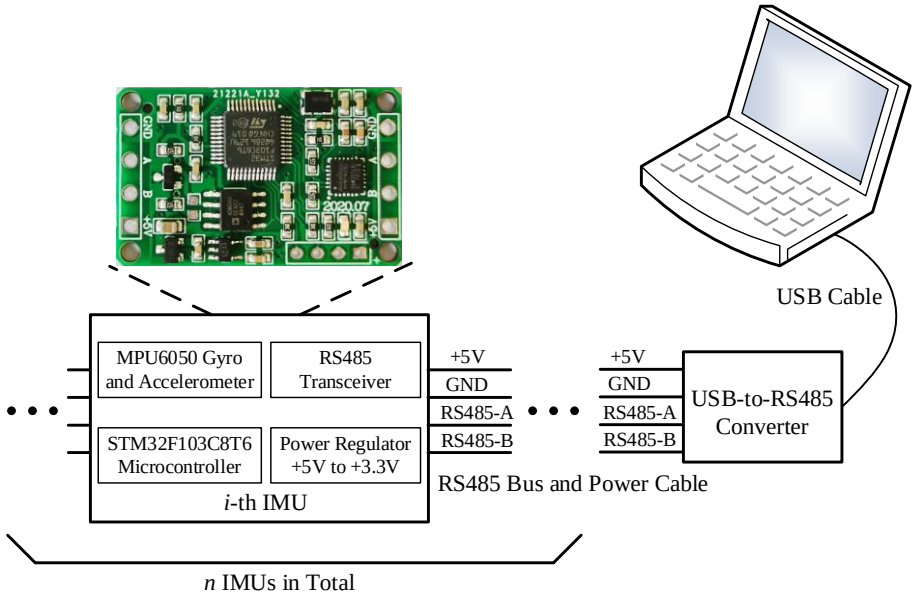

Fig. 4 Architecture of the measurement system.

The IMU shown in Fig. 4 is a custom-made sensor module using the latest off-the-shelf devices. The onboard MEMS inertial sensor is MPU6050 that integrates a tri-axis gyroscope and a tri-axis accelerometer on a single chip. The sensor readings are accessed via a I2C interface by a microcontroller STM32F103C8T6 that features a 32-bit ARM Cortex-M3 core running at 72

MHz. The +5 V power supply from the USB port is regulated to +3.3 V using a low dropout regulator MIC5207. A half-duplex RS485 transceiver ADM3485 converts the logic level UART signals into RS485 differential level signals. It is worth noting that the cost of the IMU is low because common electronic components are used.

III. Experimental Results and Discussion

A. Experimental Setup

Experimental assessment of the measurement system was conducted on a purpose-built test rig, as shown in Fig. 5. An elastic steel strip with a dimension of 2060 mm × 40 mm × 1.2 mm (length × width × thickness) is used to simulate the cross-sectional shape of the rubber dam. A total of 11 IMUs are attached to the strip with an equal spacing of 200 mm, so the center-to-center distance between the first and last IMUs along the steel strip is 2000 mm. The strip is fixed to a guide rod via two bearing blocks at both ends. As shown in Fig. 5(b), the distance between the two bearing blocks capable of sliding on the rod can be adjusted, which simulates the adjustment of the base width or the distance between anchor bolt lines of the rubber dam. The inclination of the steel strip at both ends can also be adjusted using rotation shafts shown in Fig. 5(b), which simulates the adjustment of the rising angles at upstream and downstream sides of the rubber dam. The experimental setup allows the elastic steel strip to be bended into different shapes, simulating the shapes of the rubber dam under different upstream water level, downstream water level and internal pressure conditions.

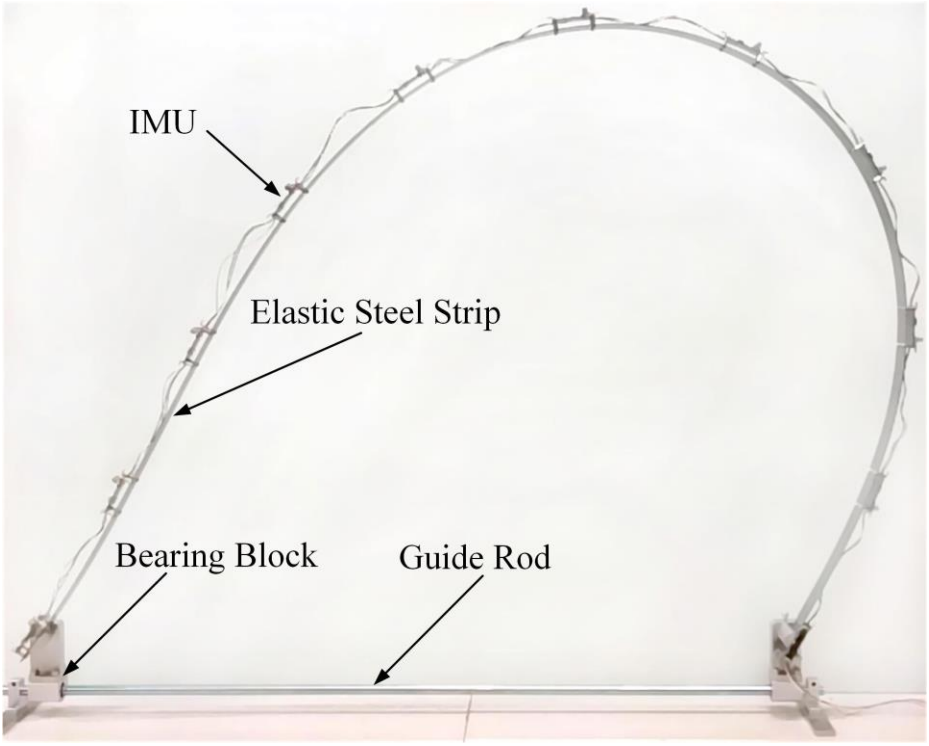

(a) Test rig

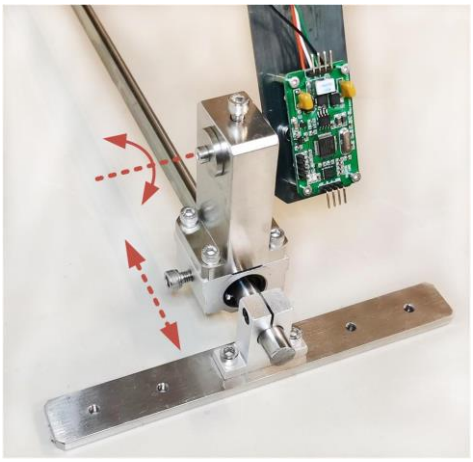

(b) Mechanism for adjusting base width and rising angles

(c) Digital camera

Fig. 5 Experimental setup.

In order to evaluate the shape measurement results quantitatively, a digital camera shown in Fig. 5(c) was used to capture the image of the test rig. The camera is mounted approximately on the central axis of the test rig using a tripod from a distance of 1.9 m. The digital images are processed using MATLAB and the steel strip is identified based on the color information. The

dimension of the steel strip is measured quantitatively with the aid of an object with known dimensions in the image. After calibration, the uncertainty of the camera for dimensional measurement is 2.6 mm. The measurement results from the IMU array are compared against those from the digital camera.

B. ***Shape Measurement Results***

The IMU array was first tested under static conditions. Fig. 6 shows a typical shape measured using both the IMU array and the camera. As illustrated, the measurement results from the IMU array and the camera agree well with each other. For quantitative assessment of the results, a similarity index is defined by the following equation:

$$SI = \frac{A_{diff}}{A_{ref}} \times 100\% \tag{15}$$

where A_{diff} represents the area between the two shape curves measured using the IMU array and the camera, and A_{ref} represents the area of the reference shape, i.e. the area encircled by the horizontal axis and the shape curve measured using the camera, as illustrated in Fig. 6. The similarity index is zero when the two shapes are exactly the same and overlap each other, and it may exceed 100% if the measured and reference shapes differ significantly. Therefore, the measurement error can be quantified using the similarity index defined by equation (15). For the shape measurement results in Fig. 6, the similarity index is 3.74%. Another quantity that can be used to assess the shape measurement result is the mismatch distance between the measured and true locations of the last IMU, which should ideally be zero. In Fig. 6, the mismatch distance is 12.3 mm, which is very small in comparison with the dimension of the shape. In addition, the height of the rubber dam is an important parameter to be controlled. The relative error of height measurement is -2.44%. The three criteria just mentioned should be used jointly in order to

quantify the shape measurement result comprehensively, as one of them alone can only represents one facet of the result. It should be noted that the shape measured using the camera is not exactly the real shape of the steel strip, mainly because of the optical and perspective distortions of the camera [28]. Although the camera induces errors for quantitative assessment, it can serve as a convenient, low cost and sufficiently accurate reference measuring device. Moreover, the shape measurement result has been considerably improved in comparison with those in [25], because the rising angles on both sides have been measured using the first and last IMUs, respectively.

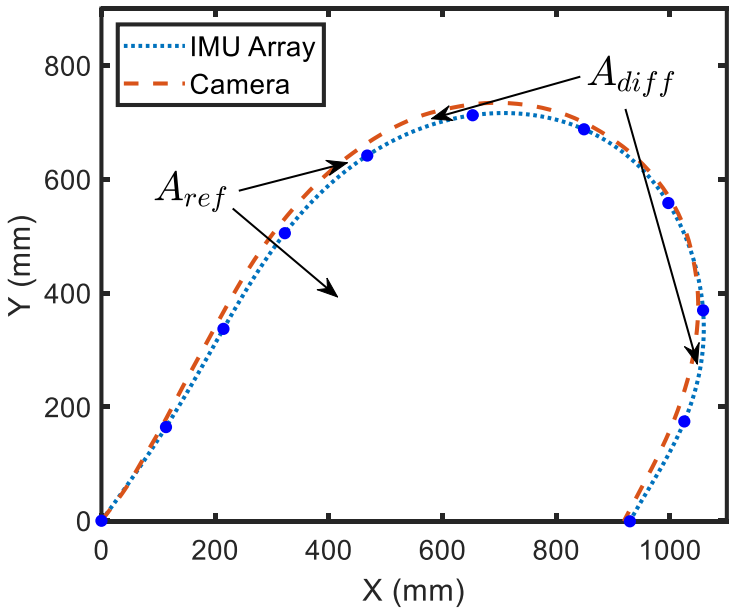

Fig. 6 Shapes measured using the IMU array and the camera under static conditions. The locations of the IMUs are indicated using blue blobs.

As described above, one shortcoming of the inertial sensing method for shape measurement is that the measurement error of one IMU node influences the shape after this node because of the integration operation in equation (14). It is vital that all IMU nodes measure the tangent angles accurately in order to obtain a reliable measurement result. If one node fails or works abnormally, the reading of this node should be discarded. Therefore, the influence of node elimination from

the array on the shape measurement result was investigated. Fig. 7 shows the shapes reconstructed without using one, three and five IMU nodes, respectively. As can be seen, when a few or even nearly half of the nodes are eliminated, the shape measurement result is affected only slightly. It is also obvious that the three measurement criteria, i.e. similarity index, mismatch distance of the last node and relative error of height are similar under the three conditions. The above result stems from the fact that the tangent angle varies almost linearly along majority of the circumference of the rubber dam, as illustrated in Fig. 3(b). If the shape is very complex and the tangent angle varies nonmonotonically, elimination of some IMU nodes would lead to significant errors. More IMU nodes not only help increase the measurement accuracy but also provide redundancy and fault tolerance, but a trade-off has to be made between these benefits and cost, system complexity as well as update rate that is subject to the communication bandwidth of the RS485 bus.

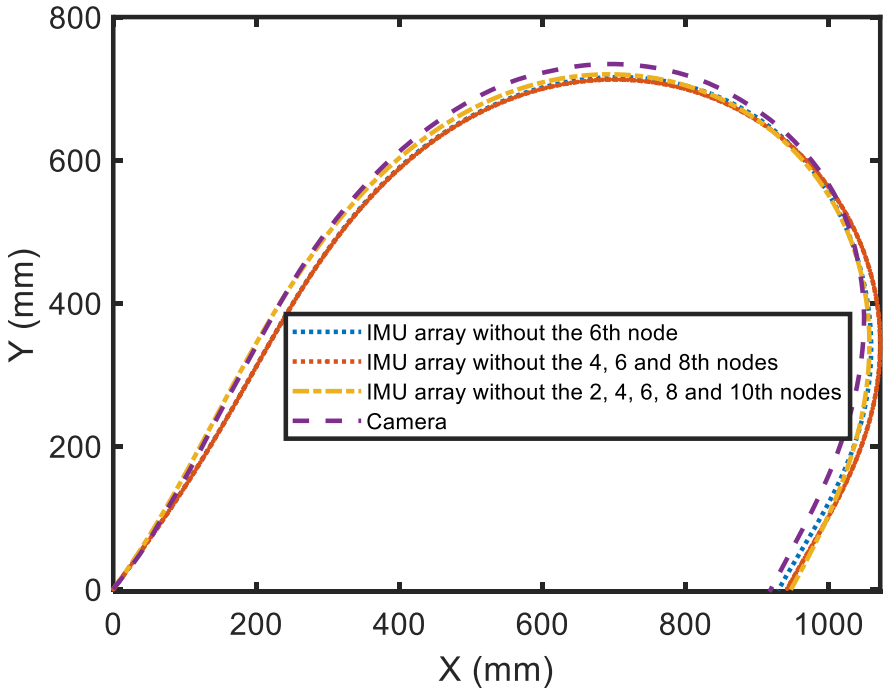

Fig. 7 Shapes measured without using some IMU nodes.

The effectiveness of the adaptive complementary filter for shape measurement under dynamic conditions was also investigated experimentally. Two orientation estimation algorithms were executed simultaneously on the IMU, with one using only the accelerometer (algorithm described by equation (5)) and the other using both the accelerometer and the gyroscope for sensor fusion (algorithm described by equations (9) and (10)). In addition, the video stream from the digital camera was integrated into the console program using the free OpenCvSharp library [29], which takes snapshots of the steel strip when the broadcast command is issued to the RS485 bus. In this way, the shapes measured using the accelerometer array, the IMU array and the camera at the same instant can be obtained. Fig. 8 shows the measurement results in half of a vibration period when the steel strip was shaken manually at a frequency of approximately 0.8 Hz. Table I presents the three measurement criteria for the four instants in Fig. 8. As can be seen, the shape measurement results using the IMU array under dynamic conditions degenerate considerably in comparison with those obtained under static conditions. The results from the accelerometer array are much worse than those from the IMU array due to lack of the compensation mechanism for external acceleration. The shapes measured using both accelerometer and IMU arrays at 0.0 s and 0.6 s resemble the reference shape more closely than those at 0.2 s and 0.4 s when the vibration speed is higher. For industrial application, the measurement results from the accelerometer array are unacceptable because of the large measurement errors.

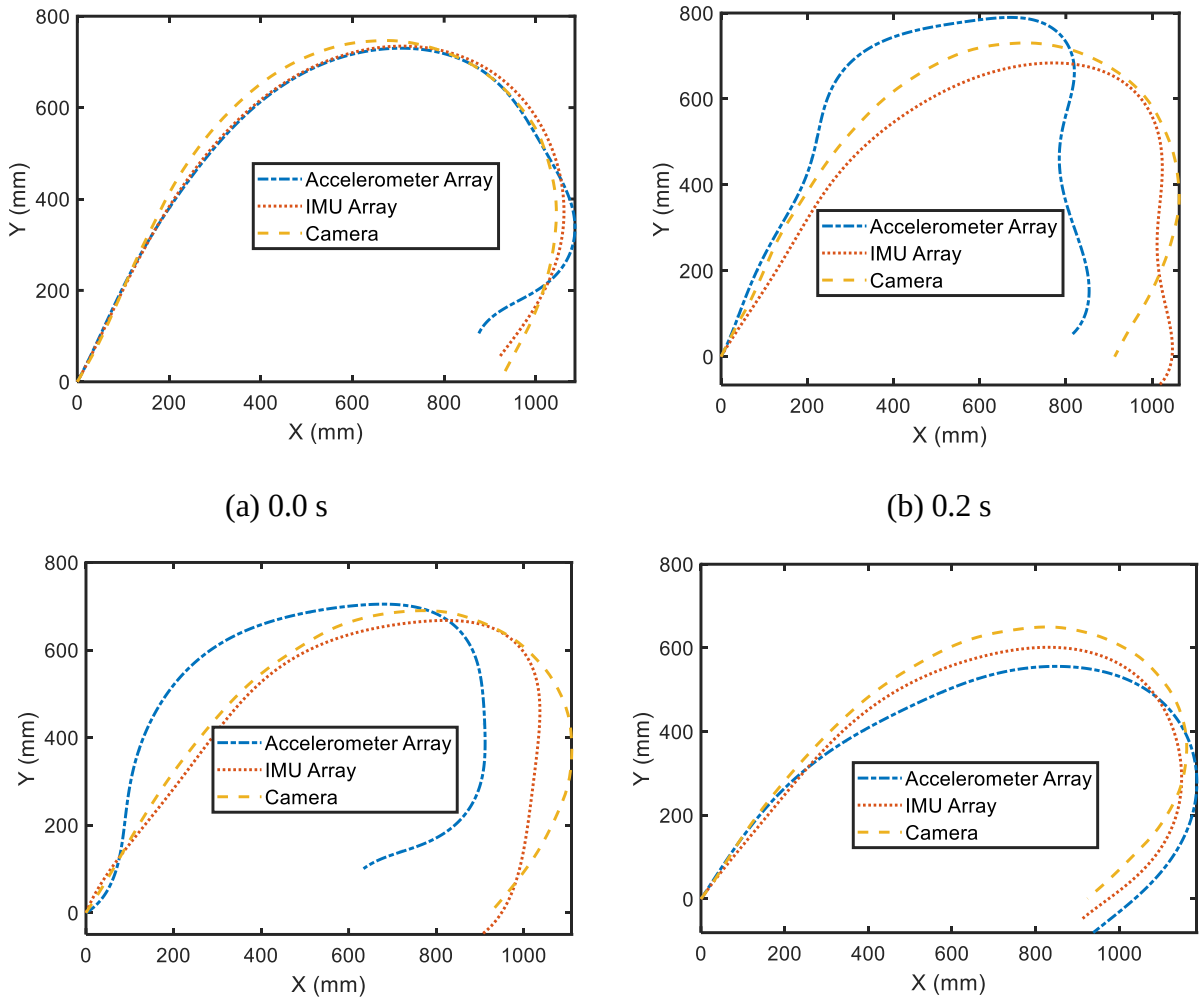

(a) 0.0 s (b) 0.2 s

(c) 0.4 s (d) 0.6 s

Fig. 8 Shapes measured using the accelerometer array, the IMU array and the camera under a dynamic condition.

Table I. Measurement criteria for the four instants in Fig. 8.

Time instant	Sensor array	Similarity index	Mismatch distance (mm)	Relative error of height
0.0 s	Accelerometer	6.10%	107.5	-2.26%
	IMU	3.95%	46.5	-1.65%
0.2 s	Accelerometer	33.87%	110.8	8.11%
	IMU	10.29%	123.0	-6.40%
0.4 s	Accelerometer	58.95%	304.0	2.15%
	IMU	4.61%	46.4	-3.23%
0.6 s	Accelerometer	36.88%	82.6	-14.48%
	IMU	8.50%	49.1	-7.47%

It is also feasible to reconstruct the shape by starting the integration from arc length L where

the 11-th IMU node is located instead of arc length 0 where the first IMU node is located. The resulting shapes are the same with those shown in Fig. 8, except that they align with the reference shape at the 11-th node rather than the first one. In Fig. 8(b) and (c), the shape measurement error around the 9-th node is much larger than that around the second node. This is because the shaking force is applied at approximately the third node, and the elasticity of the strip causes complex vibration dynamics and large external acceleration around the 9-th node.

Although the uncertainty in orientation determination due to external acceleration cannot be completely eliminated using the adaptive complementary filter, which has been a long-standing problem for inertial sensors [16-24], the shape measurement results have been considerably improved by the proposed method, from which more accurate height and vibration parameters can be derived. In practice, the vibration frequency is generally lower than 0.8 Hz and therefore more accurate measurement results can be expected. Under occasional circumstances, the rubber dam may experience impacts by sediments, ice, debris and even ships. The impulsive excitation may lead to large accelerations that cause high distortion of the reconstructed shape. Therefore, the smart condition monitoring system should be able to assess the quality of the shape and height measurement results based on the magnitude of external accelerations.

C. ***Discussion***

The measurement system will work in harsh underwater environments. Replacement of faulty sensor nodes is extremely difficult, if not impossible. Therefore, the validity of the sensor readings should be checked using some algorithm in order to avoid erroneous sensor readings to be used for shape reconstruction, as mentioned above.

A practical issue when using the IMU array fixed on the rubber dam for shape reconstruction is the elongation of the rubber material, which causes uncertainty in the distance between IMU

nodes. In order to reduce the uncertainty, the true distance will be estimated using the material properties of the rubber sheet (e.g. Young's modulus and thickness) as well as the tension in the material calculated using hydrostatic models [2, 26].

Reliability is a major concern when scaling up the laboratory prototype to a full-scale industrial measurement system in the field, as rubber dams are safety critical hydraulic structures. A series of testing will be performed to discover potential problems in the field, such as electromagnetic compatibility (EMC) testing, ingress protection (IP) testing, thermal testing, etc.

IV. CONCLUSION

This paper has presented an inertial sensing based method to measure the cross-sectional shape of an inflatable rubber dam. Accelerometer and gyroscope measurements have been adaptively combined to improve orientation estimation under dynamic conditions. A continuous tangent angle function derived by interpolating the measured tangent angles at discrete locations has been numerically integrated to reconstruct the cross-sectional shape. Experimental results obtained have demonstrated that the measured shape agrees well with the reference one under a typical static condition, with a similarity index of 3.74%, mismatch distance of the last IMU node being 12.3 mm and relative error of height measurement being -2.44%. Due to the presence of external acceleration under dynamic conditions, the similarity index increases to 10.29%, the mismatch distance of the last IMU node reaches 123.0 mm and the relative error of height measurement increases to -7.47% when the test rig vibrates at a frequency of approximately 0.8 Hz. Nevertheless, the measurement results from the IMU array have been considerably improved in comparison with those from the accelerometer array. In addition, the measurement system has been demonstrated to be robust against node failure if erroneous IMU readings are identified and

excluded from shape reconstruction. In future, field trials will be carried out to assess the performance and operability of the measurement system in a real environment.

ACKNOWLEDGMENT

This work was supported by Innovate UK under a KTP Grant 1025486.

REFERENCES

[1] X. Q. Zhang, P. W. M. Tam, and W. Zheng, "Construction, operation, and maintenance of rubber dams," Canadian Journal of Civil Engineering, vol. 29, no. 3, pp. 409-420, 2002.

[2] M. Streeter, L. Rhode-Barbarigos, and S. Adriaenssens, "Form finding and analysis of inflatable dams using dynamic relaxation," Applied Mathematics and Computation, vol. 267, pp. 742-749, 2015.

[3] M. Gebhardt, "On the causes of vibrations and the effects of countermeasures at water-filled inflatable dams," Proceedings of the First European Congress of the IAHR, Edinburgh, UK, May 4-6, 2010.

[4] S. Zhang, "High-speed 3D shape measurement with structured light methods: A review," Optics and Lasers in Engineering, vol. 106, pp. 119-131, 2018.

[5] Z. Wang, "Review of real-time three-dimensional shape measurement techniques," Measurement, vol. 156, p. 107624, 2020.

[6] T. L. T. Lun, K. Wang, J. D. L. Ho, K. H. Lee, K. Y. Sze, and K. W. Kwok, "Real-time surface shape sensing for soft and flexible structures using fiber Bragg gratings," IEEE Robotics and Automation Letters, vol. 4, no. 2, pp. 1454-1461, 2019.

[7] J. Hoffman, D. H. Waters, S. Khadka, and M. S. Kumosa, “Shape sensing of polymer core composite electrical transmission lines using FBG sensors,” IEEE Transactions on Instrumentation and Measurement, vol. 69, no. 1, pp. 249-257, 2020.

[8] T. L. T. Lun, K. Wang, J. D. L. Ho, K. Lee, K. Y. Sze, and K. Kwok, “Real-time surface shape sensing for soft and flexible structures using fiber Bragg gratings,” IEEE Robotics and Automation Letters, vol. 4, no. 2, pp. 1454-1461, 2019.

[9] G. Saggio, F. Riillo, L. Sbernini, and L. R. Quitadamo, “Resistive flex sensors: a survey,” Smart Materials and Structures, vol. 25, p. 013001, 2016.

[10] A. Rashid and O. Hasan, “Wearable technologies for hand joints monitoring for rehabilitation: a survey,” Microelectronics Journal, vol. 88, pp. 173-183, 2019.

[11] G. D. Voinea, S. Butnariu, and G. Mogan, “Measurement and geometric modelling of human spine posture for medical rehabilitation purposes using a wearable monitoring system based on inertial sensors,” Sensors, vol. 17, no. 1, doi: 10.3390/s17010003, 2017.

[12] A. Dementyev, H. L. C. Kao, and J. A. Paradiso, “SensorTape: modular and programmable 3D-aware dense sensor network on a tape,” Proceedings of the 28th Annual ACM Symposium on User Interface Software & Technology, pp. 649-658, Charlotte, NC, USA, November 11-15, 2015.

[13] A. Hermanis, R. Cacurs, and M. Greitans, “Acceleration and magnetic sensor network for shape sensing,” IEEE Sensors Journal, vol. 16, no. 5, pp. 1271-1280, 2016.

[14] T. Stanko, S. Hahmann, G. Bonneau, and N. Saguin-Sprynski, “Shape from sensors: Curve networks on surfaces from 3D orientations,” Computers & Graphics, vol. 66, pp. 74-84, 2017.

[15] S. Nathalie, D. Dominique, L. Bernard, and B. Luc, “Curve reconstruction via a ribbon of sensors,” Proceedings of the 14th IEEE International Conference on Electronics, Circuits and Systems, pp. 407-410, Marrakech, Morocco, December 11-14, 2007.

[16] Y. S. Suh, “Orientation Estimation Using a Quaternion-Based Indirect Kalman Filter With Adaptive Estimation of External Acceleration”, IEEE Transactions on Instrumentation and Measurement, vol. 59, no. 12, pp. 3296-3305, 2010.

[17] W. Li and J. Wang, “Effective adaptive Kalman filter for MEMS-IMU/magnetometers integrated attitude and heading reference systems,” Journal of Navigation, vol. 66, no. 1, pp. 99-113, 2013.

[18] A. Makni, H. Fourati, and A. Y. Kibangou, “Energy-aware adaptive attitude estimation under external acceleration for pedestrian navigation,” IEEE/ASME Transactions on Mechatronics, vol. 21, no. 3, pp. 1366-1375, 2016.

[19] T. S. Yoo, S. K. Hong, H. M. Yoon, and S. Park, “Gain-scheduled complementary filter design for a MEMS based attitude and heading reference system,” Sensors, vol. 11, pp. 3816-3830, 2011.

[20] J. Calusdian, X. Yun, and E. Bachmann, “Adaptive-Gain Complementary Filter of Inertial and Magnetic Data for Orientation Estimation,” Proceedings of 2011 IEEE International Conference on Robotics and Automation, pp. 1916-1922, Shanghai, China, May 9-13, 2011.

[21] X. Shen, M. Yao, W. Jia, and D. Yuan, “Adaptive complementary filter using fuzzy logic and simultaneous perturbation stochastic approximation algorithm,” Measurement, vol. 45, pp. 1257-1265, 2012.

[22] B. Fan, Q. Li, and T. Liu, "Improving the accuracy of wearable sensor orientation using a two-step complementary filter with state machine-based adaptive strategy," Measurement Science and Technology, vol. 29, p. 115104, 2018.

[23] A. R. P. Andrien, D. Antunes, M. J. G. van de Molengraft, and W. P. M. H. Heemels, "Similarity-based adaptive complementary filter for IMU fusion," Proceedings of 2018 European Control Conference, pp. 3044-3049, Limassol, Cyprus, June 12-15, 2018.

[24] P. Narkhede, A. N. J. Raj, V. Kumar, V. Karar, and S. Poddar, "Least square estimation-based adaptive complimentary filter for attitude estimation," Transactions of the Institute of Measurement and Control, vol. 41, no. 1, pp. 235-245, 2019.

[25] Y. Hu, Y. Yan, C. Efstratiou, and D. Vela-Orte, "Quantitative shape measurement of an inflatable rubber dam using inertial sensors," Proceedings of 2020 IEEE International Instrumentation and Measurement Technology Conference, Dubrovnik, Croatia, May 25-28, 2020.

[26] A. A. N. Alhamati, T. A. Mohammed, J. Norzaie, A. H. Ghazali, and K. K. Al-Jumaily, "Behavior of inflatable dams under hydrostatic conditions," Suranaree Journal of Science and Technology, vol. 12, no. 1, pp. 1-18, 2005.

[27] A. Pressley. Elementary Differential Geometry, 2nd Edition. Springer -Verlag London Limited, 2010.

[28] Z. Tang, R. G. von Gioi, P. Monasse, and J. Morel, "A precision analysis of camera distortion models," IEEE Transactions on Image Processing, vol. 26, no. 6, pp. 2694-2704, 2017.

[29] OpenCvSharp: .NET Framework wrapper for OpenCV. Available online: https://github.com/shimat/opencvsharp, accessed on July 6, 2020.